

We are IntechOpen, the world's leading publisher of Open Access books Built by scientists, for scientists

6,900

Open access books available

186,000

International authors and editors

200M

Downloads

Our authors are among the

154

Countries delivered to

TOP 1%

most cited scientists

12.2%

Contributors from top 500 universities



WEB OF SCIENCE™

Selection of our books indexed in the Book Citation Index
in Web of Science™ Core Collection (BKCI)

Interested in publishing with us?
Contact book.department@intechopen.com

Numbers displayed above are based on latest data collected.
For more information visit www.intechopen.com



Fatigue Crack Resistance of Ultrafine-Grained Copper Structures

Luca Collini

*Department of Industrial Engineering, University of Parma
Italy*

1. Introduction

In the last 25 years, we have witnessed to an increasing interest in developing and characterising the so-called micro- and nano-scale classes of structural materials. Micro- and nano-materials, which have arrangements, grain structures and sub-structures of less than one micron, present mechanical properties better than those belonging to the original materials (Valiev, 1997; Valiev et al., 2000). In general, since the grain size ranges between 0.1 and 1 μm , such materials are designated as ultrafine-grained (UFG) materials.

Nowadays, UFG materials have many technological applications. Due to their outstanding mechanical properties they can be successfully employed in aircraft construction as well as for high performance tools. The highly localised shear in the grain refinement process enhances their behaviour, when used as a simple plastic joint and when employed as self-sharpening tools. There are two main methods to produce UFG metals. The so-called “bottom-up” approach of synthesis, by which atoms, molecules and nanoparticles participate in order to build blocks for the creation of complex structures. Alternatively, there is the “top-down” process in which a hard solid-state elaboration of materials occur. In this approach, coarse-grained materials are refined into nanostructured materials through heavy straining or shock loading. In particular, as the market asks more and more for UFG, researchers must answer the big questions related to the complete identification of their mechanical behaviour.

Presently, the most studied nanomaterials are titanium, aluminium and copper alloys, which are also those mainly considered in this work. The ultrafine-grained Copper (UFG-Cu) structure is obtained from coarse-grained Copper (CG-Cu), from which it maintains the FCC crystallographic system, through different techniques. Among these, the most popular are electrodeposition, mechanical alloying, and severe plastic deformation (SPD) techniques. This last class of technique belongs to the Equal Channel Angular Pressing (ECAP) method, which consists of the cold refinement of the grain structure, obtained by the repeated passage of a material billet through an angular die (Valiev & Langdon, 2006). One can observe that, as it can be seen in Fig. 1, the UFG-Cu obtained from an increasing number of ECAP passages tendentially presents a structure made up of equiaxed grains, but of a medium size and strongly reduced with respect to the original CG-Cu. In fact, the resulting structure is composed of grains of different sizes, and it is important to note that the presence of larger grains still provides ductility to the material (Wei & Chen, 2006).

To give an appropriate and complete description of the advanced characteristics of this class of materials, in line with the technological and process research, much work has still to be done in the characterisation of the mechanical properties of UFG structures, especially in those concerning fatigue and crack propagation resistance. Furthermore, fracture mechanisms and damage evolution have yet to be fully understood. Some relevant works describing studies on nanomaterials are those presented in Meyers et al. (2006) and Valiev (1997), while others focused on the investigation of the fatigue and the fatigue crack resistance of UFG-Cu are Lugo et al. (2008), Höppel et al. (2006), Cavaliere (2009), Lukáš et al. (2009), Vinogradov (2007) and Collini (2010a, 2010b).

First of all, one cannot disregard the size effect derived from the intense refining of the grains in the material: in fact, in reducing the typical sizes of the structure below one micron, new deformation mechanisms will be taking place and this leads to behaviours that are different from those characteristic of the CG structures. In particular, the size effect is due to the formation of new types of dislocation such as the Geometrically Necessary (GNDs) type, and it causes a shifting from the Hall-Petch relation, and furthermore plastic deformation does not appear uniform for such a small structure. More relevant, is that the constitution and the interaction between the grain interior regions and the grain boundary regions assumes an increasing importance as the typical sizes of the structures decrease, because the grain boundary gradually becomes thicker and represents a stiff wall around the inside of the grain, in which even changes to the mechanisms of the dislocations pile-up (Kozlov et al., 2004).

The aim of the hardening process in a metal, i.e. of the increasing of the local plastic deformation energy, is to increase the amount of energy that forces a dislocation to move inside a single grain (pile-up mechanism), and from one grain to another crossing a grain boundary. In fact, the higher the stress needed to invoke the dislocation movement, the higher the yield strength of the metal. This is why the dislocation hardening produced by grain refinement brings a considerable enhancement in static and fatigue strength, and of the hardness of metals (Thomson & Backofen, 1971; Meyers et al., 2006; Mughrabi et al., 2004).

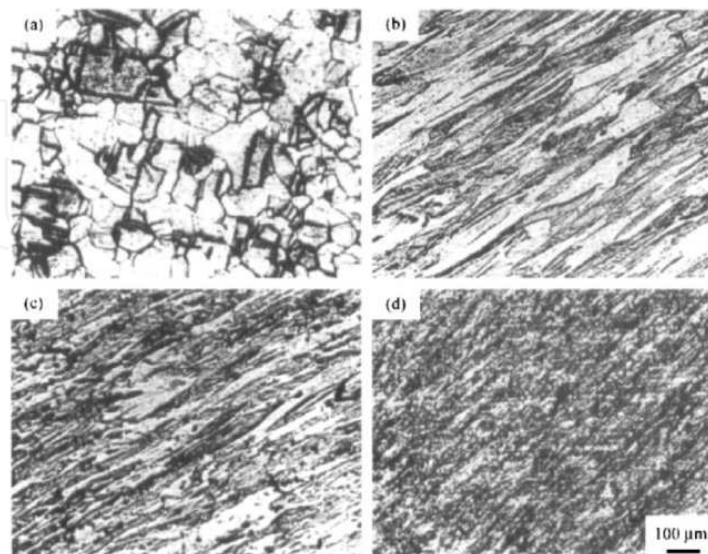


Fig. 1. Microcrystalline structure of copper: (a) before and (b-d) after 8, 10 and 12 ECAP passages (Wei & Chen, 2006).

The effect of the grain size on the cyclic plasticity and fatigue life of metals has been the focus of many investigations on steel, copper, nickel, titanium and magnesium based alloys. In general, two major conclusions based on these studies have been drawn: (i) the fatigue limit of pure f.c.c. metals with relatively high stacking fault energy and wavy slip behaviour is not affected by the grain size; and (ii) the fatigue strength of materials exhibiting planar slip, increases with decreasing grain size and follows the Hall-Petch relationship in the same way as the yield stress in conventional polycrystalline metals (Vinogradov, 2007). In particular, the studies concerned with UFG copper have shown the following aspects: 1) the UFG copper exhibits higher fatigue strength than the coarse-grained (CG) counterpart when the cycling is stress-controlled (Kunz et al., 2006), and presents lower fatigue strength during strain-controlled testing (Höppel et al., 2006); 2) a low purity UFG copper alloy shows higher resistance in its overall fatigue life (Xu et al., 2008); 3) the level of purity affects the fatigue behaviour (Lukáš et al., 2009). It has been found that the ECAP route also affects fatigue strength. Both the effects (purity and route) are more pronounced at low stress amplitudes.

A large number of studies have been conducted on the static and fatigue properties of UFG copper, but up until now very little data on the fatigue crack growth (FCG) behaviour of this material are available. This is mainly due to the difficulty in obtaining quite large bulk volumes of an ECAPed material to be machined in standard specimens for crack propagation tests. However, knowledge of FCG behaviour is of crucial importance for most engineering applications, and it is necessary for a comprehensive understanding of the fatigue properties.

Experimental fatigue crack propagation curves for the UFG copper can be found in the literature (Vinogradov, 2007; Cavaliere, 2009; Horiky et al. 2011). These works show that UFG materials exhibit the same crack propagation behaviour as polycrystals, i.e. a threshold regime, an intermediate stable growth regime well described by the Paris-Erdogan law, and an instable regime at high crack growth rates. In UFG Ni, the growth rate of a defect in the threshold regime is higher in a UFG alloy than in that of the polycrystalline reference material (Hanlon et al., 2005). This behaviour has been ascribed to the absence of a tightening mechanism in the UFG state, e.g. roughness of the crack path, due to its peculiar microstructure. Indeed, in UFG microstructures the crack path usually appears as straight and smooth, providing faster growth rates under limited crack tip plasticity. A prevalence of intergranular fracture modes during FCG was experimentally observed, explaining the nearly straight crack path in a uniform UFG structure. However, direct in-situ observation of the initiation and growth of a small, semi-elliptical surface cracks in a UFG copper structure has shown a transition of the propagation mechanism after about 0.1 mm of crack length: as the schematic in Fig. 2 illustrates. From intergranular and straight, the crack path becomes tortuous with a decrease in the FCG rate when the cyclic plastic zone (CPZ) ahead of the crack tip involves quite a large number of grains (Goto et al., 2009). This change in the propagation mechanism is due to the interrelationship between the grains' structure and the crack. Another work on high-purity UFG copper prepared by high pressure torsion (HPT) shows that the resistance to crack initiation is increased by the grain refinement, but that the stability of the microstructure during cycling is of utmost importance (Horiky et al. 2011).

However, a deeper understanding of the resistance of ultrafine-grained structures is necessary, in particular about the propagation of long, well-developed cracks, and open questions remain about the role of the reverse plastic zone at the crack tip, the shear bands formation mechanism and their interaction with the specific, small-scale granular structure, and possible toughening mechanisms.

In this chapter, the fatigue crack growth resistance of a copper alloy in the UFG state with a commercial purity level will be presented and discussed, in the light of recent findings. Results of the laboratory activity are juxtaposed with data from technical literature referring to coarse and ultrafine copper with different purity levels. A discussion on the propagation mechanisms will be conducted with the support of simplified closure and toughening models derived from the SEM analysis of crack paths.

2. Effect of grain size in crack propagation resistance

A decrease in grain size of metals and alloys generally results in an increase in strength. Improved ultimate tensile strength and yield strength does not necessarily mean that the fine-grained materials also exhibit better properties with respect to their resistance against damage by fatigue crack growth.

Propagation of long cracks in conventionally grained Cu can be well described by linear fracture mechanics. There is a good correlation between the crack propagation rate, da/dN , (a is the crack length and N number of cycles) and the stress intensity factor K . The experimentally determined crack propagation curve for stress symmetrical loading is shown in Fig. 3. The crack rate was determined on sheet centre-cracked tension specimens manufactured from Cu of 99.99 % purity. The cycling was conducted under load-controlled conditions. It is evident that the grain size influences the crack rate. Cracks in the fine-grained Cu with a grain size of 70 μm propagate faster than in the coarse-grained Cu with a grain size of 1.2 mm (Lukáš & Kunz, 1986). The experimental results in Fig. 3 can be well approximated by the equation:

$$da / dN = A(K_a^m - K_{ath}^m) \quad (1)$$

where $A = 1.1 \times 10^{-10} \text{ (mm/cycle)(MPa}\sqrt{\text{m}})^{-m}$ and $m = 7.0$ for fine-grained Cu and $A = 5.0 \times 10^{-11} \text{ (mm/cycle)(MPa}\sqrt{\text{m}})^{-m}$ and $m = 7.1$ for coarse-grained Cu. The threshold value of SIF, below which the long cracks do not propagate, is $K_{ath} = 2.1$ and 2.7 $\text{MPa}\sqrt{\text{m}}$ for fine-grained and coarse-grained Cu, respectively. From this data it is evident that from the point of view of crack propagation, the fine-grained Cu is worse than the coarse-grained.

There are a plenty of models for the propagation of long cracks. They can be divided into three basic groups: 1) models assuming that the plastic deformation in the plastic zone is the determining factor in crack growth, 2) models based on damage in front of the crack tip and 3) models based on energy considerations. The knowledge obtained from the investigation into crack propagation in Cu clearly favours those models based on the crucial role of the cyclic plastic strain at the crack tip.

In Cu of conventional grain size, a fatigue crack tip is surrounded by a dislocation cell structure in a plastic zone. An example of a dislocation structure adjacent to the long fatigue crack propagating in the Paris law region (a linear part of the da/dN vs. K_a plot in log-log coordinates) can be seen in Fig. 4. The fatigue crack was propagating in a non-crystallographic manner, macroscopically perpendicular to the principal stress. The foils for transmission electron microscopy (TEM) were prepared in the following manner. The fatigue crack surface was electrodeposited. The foils for TEM were prepared from thin slices cut perpendicularly to the macroscopic fracture surface and parallel to the crack

propagation direction. Because the crack length corresponding to the location of the foils and cyclic loads were known, it was possible to correlate the observed structure with K_a .

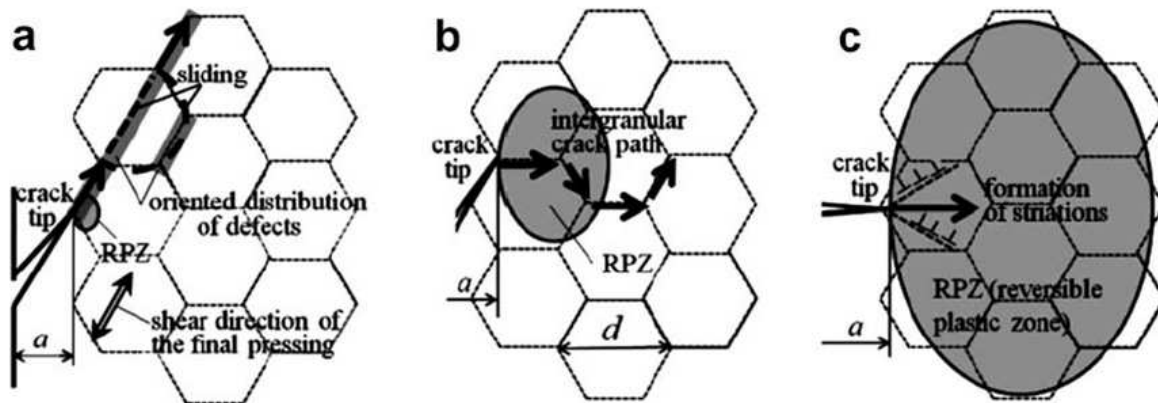


Fig. 2. Schematic of the FCG mechanism of a small surface crack in UFG Cu and of the relationship between the cyclic plastic zone (CPZ) at the crack tip and grain size: (a) when CPZ is smaller than the grain size, the crack propagates in a mechanism conforming to the local area (grain or grain boundary), e.g. along the final shear pressing direction; (b) when CPZ is 1-2 times the grain size, the crack grows along GBs where an incompatibility in deformation in adjacent grains is concentrated, showing an intergranular crack path; (c) when the CPZ is more than 3-4 times the grain size, the crack propagates due to the striation formation mechanism, associated with crack tip retardation and blunting. From Goto et al. (2009).

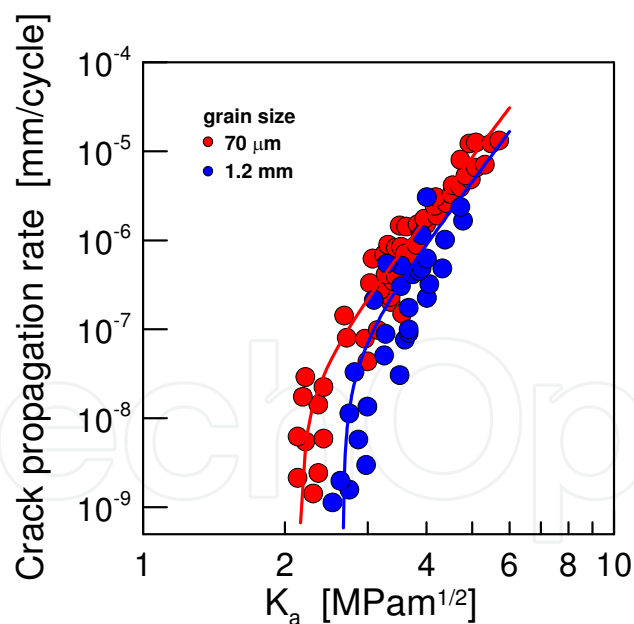


Fig. 3. Comparison of crack propagation curves for fine-grained and coarse-grained Cu.

On the left hand side of Fig. 4 the electrodeposit can be seen. On the right hand side is the well-developed cell structure, which was produced by the cyclic plastic deformation in the plastic zone. The original fatigue fracture surface can be seen in-between. Analysis of a number of TEM foils indicates that the cell size d is inversely proportional to K_a (Lukáš & Kunz, 1986).

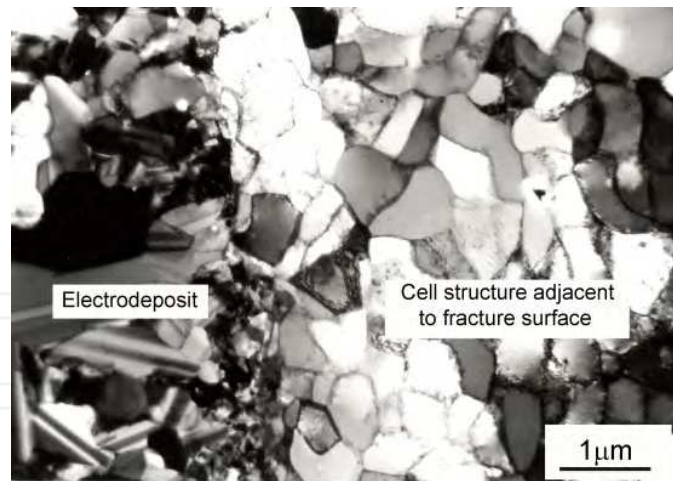


Fig. 4. Dislocation cell structure adjacent to fracture surface in conventionally grained Cu.

For the lowest crack growth rates of the order of 10^{-9} mm/cycle in the threshold region when K_a approaches K_{ath} the crack propagation mechanism in Cu changes. The crack propagates in a “zig-zag” manner and the fracture surface exhibits crystallographic features. The region of plastic zone with the cell structure is very small. TEM observations, an example is shown in Fig. 5, indicate that the crack propagates along the persistent slip bands (PSB) with a characteristic ladder-like structure. The fracture surface is straightforward and runs along the ladder. This means that at very low rates the propagating crack does not necessarily change the vein dislocation structure characteristic of the material in which the crack propagates.

Based on the observation of the dislocation structures near the crack tip in Cu, the following considerations can be made. Fig. 6 schematically illustrates the situation at the crack tip. At high crack growth rates and small grain sizes, the “fracture mechanical” plastic zone consisting of the cell structure is large compared to the length of the PSBs, which develops before the propagating crack tip. The plastic strain amplitude at the crack tip controls the crack growth process. However, for low crack growth rates and coarse-grained Cu the ratio of the length of PSBs terminating at the grain boundaries to the cell zone size increases. Some observations show that the cell zone can vanish completely. The decisive majority of the cyclic plastic strain is concentrated in the PSBs. This type of plastic zone is different from the fracture mechanical zone, which develops at loading with a high K_a . It is obvious that this effect and the effect of the grain size can substantially influence the crack growth rate.

UFG Cu produced by ECAP is typically has a grain size (cell size) of about 300 nm. This is comparable to the smallest cells observed at the tip of the fatigue crack propagating at the conditions characterized by $K_a \sim 10$ MPa \sqrt{m} (Lukáš et al., 1985). From this point of view the crack propagation resistance of UFG and CG copper in this region should be similar. Strong differences, however, can be expected in the threshold region. Here the stability of the UFG structure would play the decisive role. Horkey et al. (2011) studied the crack propagation in UFG Cu prepared by high pressure torsion. They observed very expressive grain coarsening in the vicinity of the fatigue crack in Cu of high purity. Retardation of the crack growth was reported.

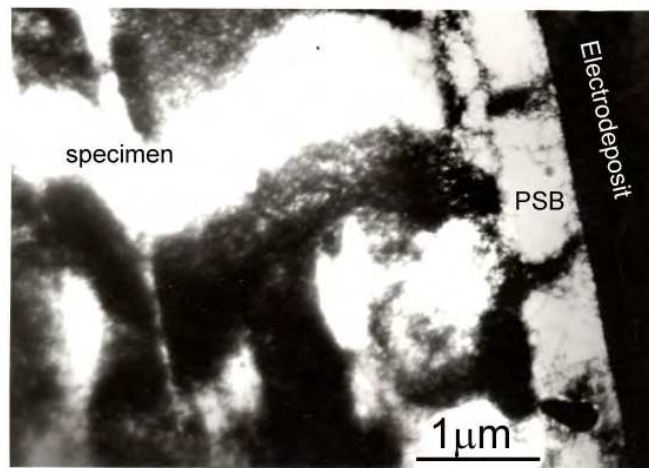


Fig. 5. Dislocation structure adjacent to the fracture surface in conventionally grained Cu created by extremely low crack growth.

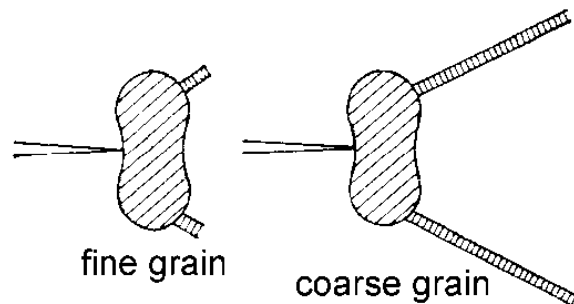


Fig. 6. Schematic representation of plastic zone in fine-grained and coarse-grained Cu.

3. Experimental methodology

3.1 Material

The material used for this study is a copper alloy, subjected to 8 passes ECAP through route Bc, i.e. with a billet rotation in the same sense rotated by 90° between each pass. The copper has been processed in the laboratory of Prof. R.Z. Valiev at the Ufa State Aviation Technical University (Russia), starting from cylindrical samples of 20 mm in diameter and 120 mm in length. Cylindrical samples of 16 mm in diameter and 100 mm in length were machined from the billets.

The microstructure obtained is shown in the micrograph of Fig. 7: the result is fine and uniform, with grain sizes ranging from 100 to 800 nm and an average size of 300 nm. The orientation map, visible in Fig. 7 on the right, shows low angle grain boundaries. The chemical composition, reported in Tab. 1, indicates that the purity, 99.90%, is of a commercial level.

The static and fatigue properties are summarised in Tab. 2, in which the properties of CG wrought copper alloy (grain size $30\ \mu\text{m}$) are also reported (Murphy, 1981). As can be seen, the ECAP process brings evident advantages to the mechanical properties: the yield strength σ_y is 4-times that of the CG, and the fatigue limit at 10^8 cycles σ_f is twice the original.

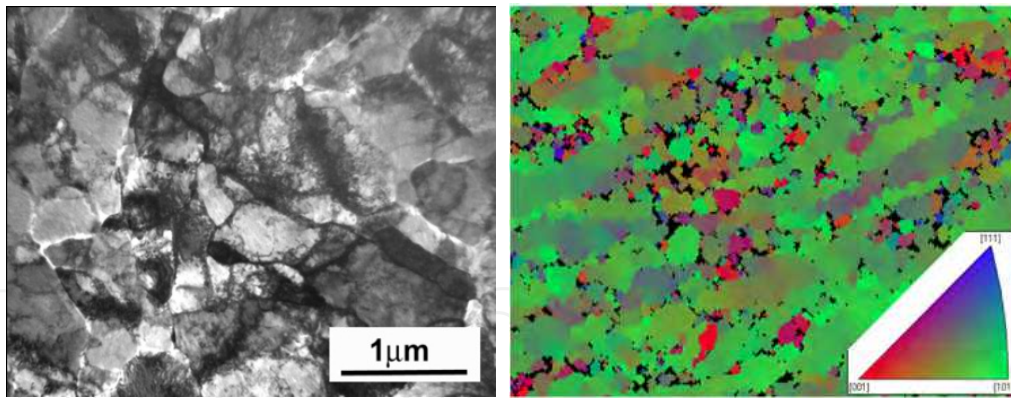


Fig. 7. TEM micrograph and grain orientation map of the ECAPed UFG copper.

Bi	Sb	As	Fe	Ni	Pb	Sn	S	O	Zn	Ag	Cu
0.001	0.002	0.002	0.005	0.002	0.005	0.002	0.004	0.05	0.004	0.003	balance

Table 1. Chemical composition (% in wt) of the UFG copper.

Structure	Grain size d_G (μm)	σ_y (MPa)	σ_u (MPa)	A%	σ_f at 10^8 cycles (MPa)
CG	30	95 \pm 5	195 \pm 5	41.5	77
UFG	0.300 \pm 0.015	375 \pm 4	387 \pm 5	18.5	168

Table 2. Mechanical properties of CG and UFG polycrystalline copper.

3.2 Procedure and data elaboration

The FCG tests were conducted in laboratory on Disk Shaped CT specimens, in air and at room temperature. A MTS 810 servo-hydraulic machine working at a frequency of 10 Hz has been used for the test. A view of the test apparatus is shown in Fig. 8.

Specimens were machined in discs of 7 mm in thickness from bars of 16 mm in diameter. The DSCT specimen is shown in Fig. 9. Due to its reduced dimensions, it has been necessary to use a Back Face Strain Measurement (BFSM) technique to monitor the crack length on the specimen, by using a very small strain gage glued to its back. In conjunction with a finite element calibration, the BFSM technique allows the calculation of the mode I Stress Intensity Factor (SIF) as a function of a/W ratio by Eq. (2):

$$K_I = \frac{P \left(2 + \frac{a}{W} \right)}{BW^{1/2} \left(1 - \frac{a}{W} \right)^{3/2}} \sum_{i=0}^4 C_i \left(\frac{a}{W} \right)^i \quad (2)$$

where P is the applied load, B and W are the characteristic specimen dimensions, and C_i is the constant relative to the DSCT geometry. The standard procedure for FCG calculation is adopted in order to realize K -increasing and K -decreasing (load-shedding) tests. Experimental tests are conducted at a load ratio $R = K_{min}/K_{max}$ equal to 0.1, 0.3, 0.5 and 0.7. The mode I crack propagation resistance is investigated both in the stable growth regime (stage II), and in the threshold regime (stage I).

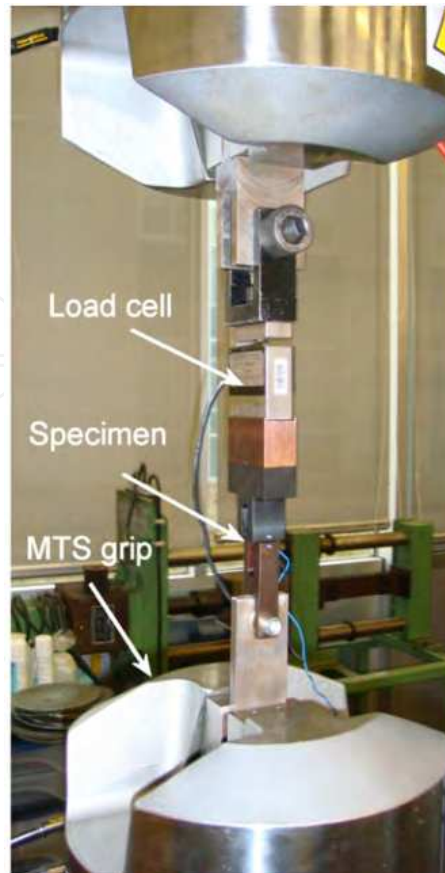


Fig. 8. FCG test apparatus.

Acquisition of each data point is automatically made every 0.1 mm of crack propagation. In order to facilitate the crack initiation and mode I crack propagation, an initial fatigue pre-cracking of 0.8 mm at load ratio 0.1 is conducted for all specimens. An estimation of ΔK_{th} at the conventional growth rate of 10^{-7} mm/cycle has been made following the procedure of regularisation. It means that data points of crack a as a function of applied ΔK , and of ΔK itself as a function of the number of cycles N , have been interpolated by exponential curves, adopting opportune values for parameters $\kappa_{1,2}$ and $\beta_{1,2}$, as indicated in Eqs. (3,4):

$$a(N) = a_0 + \kappa_1 (1 - e^{\kappa_2 N}) \quad (3)$$

$$\Delta K(N) = \Delta K_0 + \beta_1 e^{-\beta_2 N} \quad (4)$$

Deriving and plotting Eq. (3) towards ΔK points of Eq. (4), a “regularised” da/dN - ΔK curve can be obtained. From this, the threshold SIF at a conventional crack growth rate of $1 \cdot 10^{-7}$ mm/cycle is derived.

The dependence of the threshold SIF on the load ratio can be analysed by applying some classical models. For example, the linear fit proposed by Barson (1974), Eq. (5), and the power fit proposed by Klesnil and Lukáš (1972), Eq. (6):

$$\Delta K_{th} = A - BR \quad (5)$$

$$\Delta K_{th} = D(1 - R)^\gamma \quad (6)$$

are applied in this study, with opportune fitting constants A , B , D and γ .

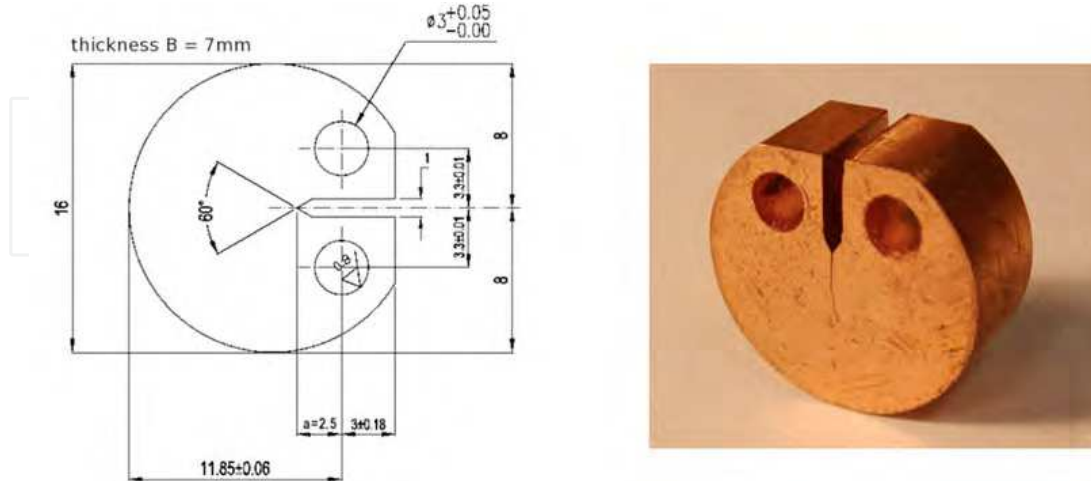


Fig. 9. The Disk Shaped CT specimen adopted for the experimentation; a propagated crack emanating from the notch is visible on the right-hand picture.

4. Fatigue crack growth resistance

4.1 Stable crack growth regime

Results of the FCG tests are now presented in the form of traditional log-log (da/dN ; ΔK) diagrams. For the sake of clarity, only one propagation curve per R -ratio is plotted.

In Fig. 10, the crack propagation in the stable regime is plotted. Other data from the literature are plotted for comparison. In particular, these are: i) FCG curve at $R = 0.25$ of pure UFG Cu ECAPed by 4Bc passes with $d_G = 270$ nm (Cavaliere, 2009); ii) FCG curve at $R = 0.5$ of UFG copper produced by 4Bc passes and $d_G = 300$ nm (Vinogradov, 2007); iii) FCG curve at $R = 0.5$ of UFG copper produced by 16A ECAP passes and $d_G = 300$ nm (Vinogradov, 2007); iv) FCG curve at $R = 0.5$ of CG copper with $d_G = 15$ μm (Murphy, 1981).

From the analysis of the data some considerations can be drawn: 1) applied ΔK ranges between $6\div 45$ $\text{MPa}\sqrt{\text{m}}$, and related FCG rates between $6 \cdot 10^{-7} \div 2 \cdot 10^{-3}$ mm/cycle, the transition from stage I to stage II is continuous, and the conventional metals points in stage II can be fitted by the classical Paris propagation law:

$$da/dN = C(\Delta K)^m \quad (7)$$

2) the load ratio at stage II influences the propagation mechanism (Fig. 10 right); 3) in stage II the propagation curves intersect around the growth rate of 10^{-5} mm/cycle.

When comparing these with previous results, one can notice that: 1) a slower FCG characterises the present UFG copper for all R -ratios; 2) the slope of the curves in the Paris regime is comparable with data from the literature, i.e. a similar crack growth mechanism is found; 3) in stage II, the present UFG Cu shows higher FCG resistance than the CG counterpart.

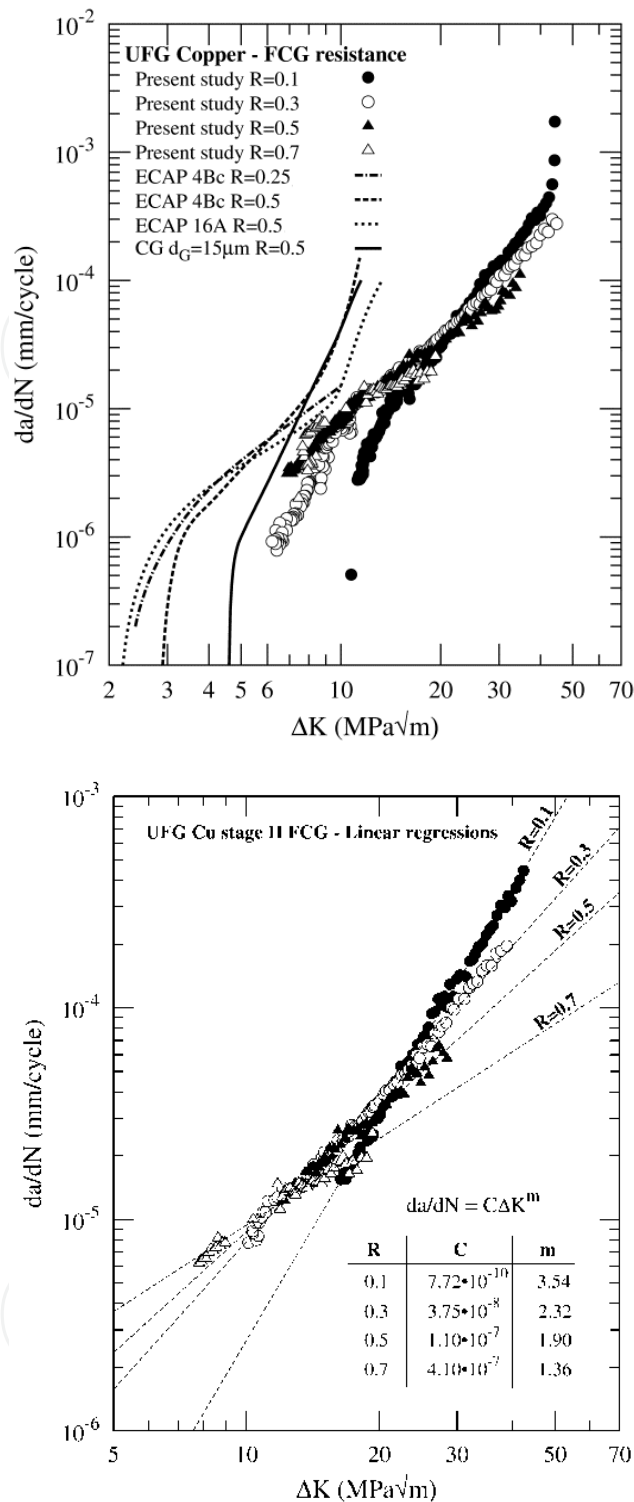


Fig. 10. FCG curves (left); linear regressions of stage II FCG rate (right).

4.2 Threshold regime (stage I)

In metals and alloys, the threshold FCG regime is usually defined by an FCG rate of around 10^{-7} mm/cycle. Since in the present tests only at $R = 0.1$ did the crack growth rate go under 10^{-6} mm/cycle, the threshold SIFs ΔK_{th} have been determined by the method reported in

section 3.2. The results are summarised in Tab. 3, and compared with ΔK_{th} values taken from the literature.

The analysis of the FCG curves near the threshold regime and values of extrapolated ΔK_{th} highlights the following. The load ratio in UFG crack propagation influences the threshold FCG regime, since the higher the R , lower the ΔK_{th} , as one can evince from Fig. 10. Moreover, the threshold SIFs are higher than values found in the literature for the same class of UFG copper, as indicated in Tab. 3 and illustrated in the trend of the C coefficient in Eq. (7) (see Fig. 11). Finally, if compared with the FCG behaviour of annealed and cold worked conventional Cu alloys, the present UFG microstructure shows a higher threshold resistance to R -ratios 0.1 and 0.3, but lower resistance when the R -ratio increases, see Fig. 12; this result is partially in contradiction to other investigations on different purity levels.

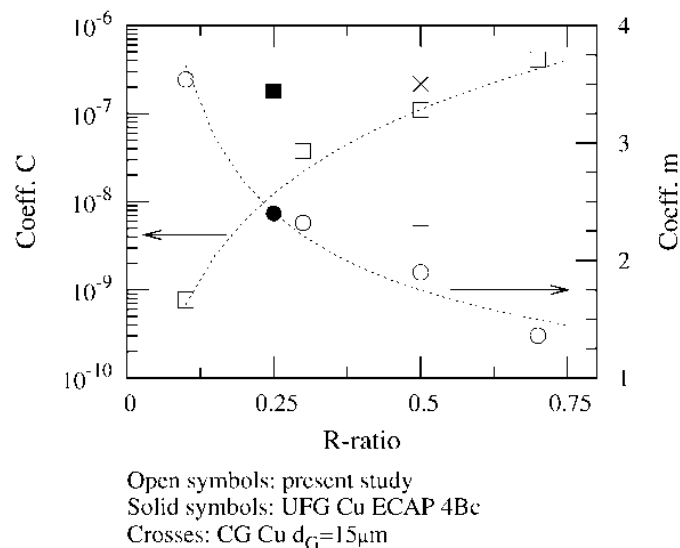


Fig. 11. Paris' law coefficient of Eq. (7) as a function of load ratio R .

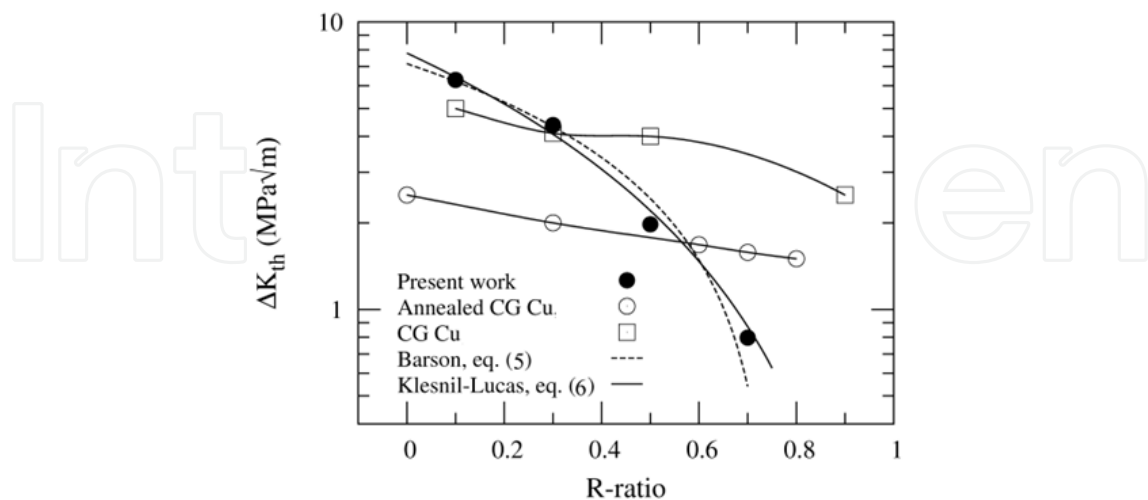


Fig. 12. Threshold stress intensity factors as a function of R -ratio.

Results of the threshold have been elaborated by Eq. (5) and Eq. (6) with the following fitting parameters: $A = 9.45 \text{ MPa}\sqrt{\text{m}}$; $B = 7.16 \text{ MPa}\sqrt{\text{m}}$; $D = 7.79 \text{ MPa}\sqrt{\text{m}}$; $\gamma = 1.82$.

R-ratio	Present UFG Cu, ECAP 8Bc	UFG Cu, ECAP 4Bc	UFG Cu, ECAP 4Bc	UFG Cu, ECAP 16A
0.1	6.3	-	4.4	2.7
0.3	4.4	2.3 (R=0.25)	-	-
0.5	2.0	-	-	-
0.7	0.8	-	-	-

Table 3. Present ΔK_{th} values and data from literature.

4.3 Discussion of results

The experimental results on FCG resistance identify two important aspects: 1) the FCG resistance of the present UFG copper is higher than that of the previously tested ECAPed copper alloys, in stage II and also in the threshold propagation regime: this can be seen in the graphs of Fig. 10 and from Tab. 3; 2) load ratio influences the threshold stress intensity factor and the mechanism of stage II crack propagation. These two aspects will now be taken into consideration.

In order to explain the relatively high crack propagation resistance of the present UFG copper, its fatigue resistance must be analysed. It has been recently shown that the fatigue strength of UFG copper with low purity is higher than that of conventional copper by a factor of 2. In particular, the copper used in Kunz et al. (2006) had the same chemical composition and ECAP processing of the present material. Its higher fatigue resistance has been justified by demonstrating the stability of the bulk microstructure during cycling, due to the stable dislocation structure and to the presence of impurities and precipitates.

The grain structure within plastic zone around the cracks was shown to differ from outside the plastic zone: the grains were found to be markedly elongated, but their size was shown to be preserved. Also, in comparison with the CG structure, a small grain size can potentially result in more homogeneous deformation, which can retard crack nucleation by reducing stress concentrations and ultimately raise the fatigue limit of the UFG structure. This has been demonstrated by other studies on ECAPed copper structures on low and high cycle fatigue (Hanlon et al., 2005; Estrin & Vinogradov, 2010).

Moreover, it can be thought that the interaction between a propagating crack and the GBs structure can produce retardation in the growth rate. In fact, in most planar slip materials, GBs provide "topological obstacles to the slip" (Vasudevan et al., 1997). This phenomenon has already been noticed and theoretical models on the crack-boundaries interaction developed, with the support of experimental evidence (Holzapfel et al., 2007; Zhai et al., 2000). In these studies, it has been shown that due to the crack-precipitate interaction at the GBs, the crack develops steps on the crack plane while bypassing the precipitates. The result is a fatigue crack retardation and deflection at a GB that, by leading to an increase in the free crack surface, produces a significant suppression of the crack propagation rate. This topological factor can be critical in the FCG behaviour of UFG metals, if one considers the huge number of GBs generated by the grain refinement process.

The analysis of the effect of the *R*-ratio on the propagation behaviour in stage II is more complicated. As can be clearly seen from Fig. 10, at a constant FCG rate propagation, a

higher R -ratio produces a slower growth rate, as if the material becomes more insensitive to the crack. This trend is not usual for polycrystalline metals, but very similar behaviour can be observed in the propagation curves of Cavaliere (2009), in which the crack growth resistance of UFG Cu alloys with increasing ECAP passes (i.e. grain refinement) are reported: going from two CG structures with 11 and 15 μm , towards UFG structures with passes 4Bc, 12Bc, 16A and 16Bc, where a lower threshold but higher stage II resistances are constantly found. The same trend is noticed in the present material when the R -ratio increases.

In order to rationalize the influence of load ratio, a crack closure approach has been attempted during the elaboration of the experimental results. The Adjusted Compliance Ratio (ACR) model (Donald, 1997) has been chosen. Depending on the ductility, FCG rate and environmental effects, numerous causes can be responsible for anticipated crack closure; among them, residual plasticity and roughness due to a tortuous crack path, characterise the so-called plasticity-induced crack closure (PICC) and roughness-induced crack closure (RICC), respectively. PICC and RICC are common mechanisms in ductile metals; PICC is mainly related to the residual plastic deformation in the steady-state FCG regime, while at threshold closure RICC is favoured by microstructural asperities of the fracture surfaces. The ACR method is based on the hypothesis that the effectively applied ΔK at the crack tip, namely ΔK_{eff} , is proportional to the strain magnitude, or to the crack tip opening displacement (CTOD), which is defined as:

$$CTOD = \frac{(1 - \nu^2) K_{max}^2}{2\sigma_y E} \quad (8)$$

The effective SIF is then calculated by correcting the applied SIF by a parameter (the ACR parameter) defined as follows:

$$\Delta K_{eff} = \Delta K \cdot ACR \quad (9a)$$

$$ACR = \frac{C_s - C_i}{C_0 - C_i} \quad (9b)$$

where C_s , C_0 and C_i are the specimen secant compliance, the compliance above the opening load and the compliance prior the initiation of the crack, respectively.

The elaboration of experimental points by this model is depicted in Fig. 13. Two main observations arise: 1) propagation curves almost overlap in stage II, and run parallel; 2) points below the $1.5 \cdot 10^{-5}$ mm/cycle show poor physical sense. It can be concluded that the ACR model rationalises the R -ratio effect in FCG stage II with discrete approximation, while it fails when applied to the threshold regime, where, as already known, the role of the microstructure achieves greater importance. This result is in partial accordance with FCG tests made on conventional CG copper, where it has been observed that by decreasing the grain size the threshold ΔK increases, suggesting that in copper crack tip plasticity considerations are more important in determining the threshold values than crack closure effects (Marchand et al., 1988).

Due of the peculiar micro-scale grain structure of UFG copper, the extension of the “process area” around the crack tip where plastic deformation concentrates can be investigated. According to Irwin, the size of monotonic and cyclic plastic zones at the crack tip can be estimated by Eq. (10) and Eq. (11) respectively:

$$r_p = \frac{1}{3\pi} \left(\frac{K_{\max}}{\sigma_y} \right)^2 \quad (10)$$

$$r_{pc} = \frac{1}{3\pi} \left(\frac{\Delta K}{2\sigma_y} \right)^2 \quad (11)$$

where σ_y is the yield stress.

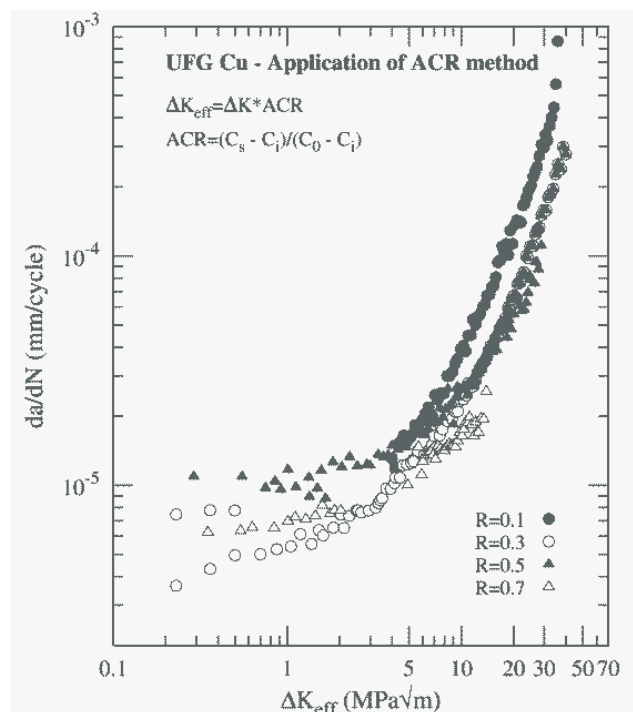


Fig. 13. Crack closure analysis by the application of the ACR model.

Results of this elaboration are shown in Fig. 14, where r_p and r_{pc} trends are reported as a function of the R -ratio, in respect to the high FCG rate ($2 \cdot 10^{-5}$ mm/cycle) and near-threshold FCG rate ($2 \cdot 10^{-7}$ mm/cycle). The same graph depicts the CTOD as calculated by Eq. (8). Fig. 14 illustrates that: 1) monotonic and cyclic plastic zones are always much wider than the characteristic microstructural dimensions (the average grain size d_G); 2) r_p and r_{pc} depend on the R -ratio in an opposite manner as a function of the FCG rate; 3) the CTOD is smaller when compared to r_p and r_{pc} . In other words, if the propagation of a fatigue crack is seen as the result of the accumulation of irreversible plastic deformation at the crack tip, in UFG copper this process involves one/two tenths of grains at a low FCG rate, but a large number of grains, up to some hundreds, at a high FCG rate.

In such a situation, one can expect a microstructure-dependent propagation mechanism at only very low FCG rates, as already observed for this material. This can partially explain the

inadequacy of the ACR closure method when applied to the threshold regime. Fig. 14 also shows that at high FCG rates the cyclic plastic zone does not depend on the R -ratio, or, equivalently, on the applied average SIF calculated by Eq. (12):

$$\Delta K_{AVG} = \frac{1+R}{1-R} \Delta K \quad (12)$$

This indicates that for an increasing ΔK_{AVG} , the monotonic plastic zone expands, while the cyclic zone stabilises, being the microstructure able to resolve the external load.

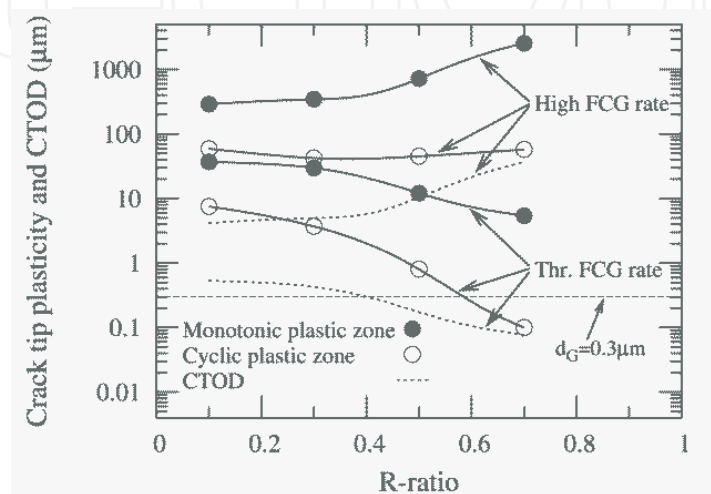


Fig. 14. Crack tip opening displacement (CTOD) and monotonic and cyclic plastic zones ahead of the crack tip calculated by Eqs. (8), (10) and (11) at $da/dN = 2 \cdot 10^{-7}$ mm/cycle and $da/dN = 2 \cdot 10^{-5}$ mm/cycle.

5. Fractographic analysis

The study of crack path and fracture surfaces is now presented to complete the analysis of the previously discussed FCG behaviour. The crack path morphology can be analysed in terms of fracture roughness R_v , measured on SEM images of cracked specimens. Roughness, that is a quantitative measure of the crack tortuosity, has been calculated by a simple graphical method, based on the superimposition of a grid on the digital image of a specimen profile.

The method is based on the counting of the profile-grid intersections, P_i , along a chosen length, L , and then expresses R_v as:

$$R_v = \frac{y}{L} \sum_i P_i \quad (13)$$

This simple technique gives a mono-dimensional estimation of roughness. R_v is calculated at different ranges of applied ΔK , for R -ratios equal to 0.3, 0.5 and 0.7. Results of the elaborations are presented in graphical form in Fig. 15. Crack tortuosity is higher when the driving force increases, but in practice it does not depend on the R -ratio. This conclusion confirms the insensitivity of the cyclic plastic zone with respect to the R -ratio at a given load range as already evidenced. Furthermore, it can be stated from Fig. 15 that R_v is only of the order of magnitude of the grain size d_G at the near-threshold regime. It means that the mechanism of fracture may only be microstructure-dependent during the threshold regime.

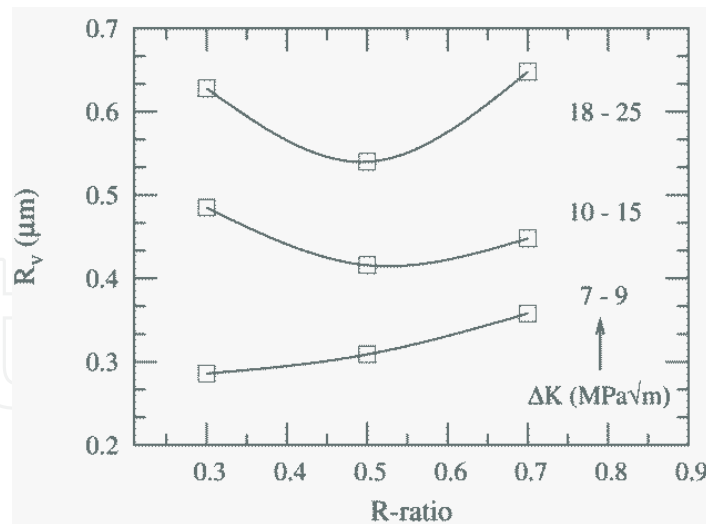


Fig. 15. Roughness of crack profile as a function of ΔK and R -ratio applied.

The fractographic analysis of the surfaces results a valuable tool to investigate the fracture mechanism and its dependence on load ratio. Some images of the crack path on the specimen profiles and of the fracture surface acquired by the SEM microscope are introduced in Figs. 16, 17 and 18.

Figs. 16 and 17 show the crack propagation profile at $R = 0.3$ and 0.7 respectively, with an increasing ΔK applied from left to right. Indications of the average SIF calculated by eq. (12) are also given. Looking at the profile morphology, an increasing tortuosity and fragmentation with an average ΔK can be seen for both R -ratios. Figs. 16(c) and 17(c), which correspond to the highest loads, show bifurcation, multi-cracking and branching of the main crack. Several small secondary cracks can be clearly seen in the perpendicular and parallel directions with respect to the main crack path direction, even at some distance from it. A very similar mechanism has been already been observed in commercially pure UFG Ti, in UFG Cu and, in AA6063 aluminium alloy.

A multi-cracking phenomenon indicates the poor capacity of the dislocation mechanism to generate around the crack tip and in the plastic wave of the hardened structure. Microcracks are generated to accommodate excessive strains in the crack vicinity, decreasing the strain hardening capability due to severe grain refinement. On the other hand, the branching mechanism may be directly responsible for the insensitivity toward crack propagation found at the stable FCG rate. During stage II, the FCG rate diminishes when R -ratio (or ΔK_{AVG}) increases, i.e. when branching becomes more evident. Indeed, it has been shown that crack deflection or multi-cracking can enhance K_{max} by a factor of about 20-30% (Vasudevan et al., 1997). This could definitely explain the FCG behaviour noticed, otherwise it would be very difficult to rationalise it with a crack closure approach.

Fig. 18 shows the fracture profile and the fracture surface near the threshold regime, at $R = 0.3$ and $R = 0.5$, respectively. The fracture morphology of Fig. 18(a), taken when the cyclic plastic zone at the crack tip was about 5-8 times the grain size, provides evidence of an intergranular mechanism, justifying the high value of ΔK_{th} found. The SEM image of Fig. 18(b) shows relatively long, straight-line (secondary) microcracks, perpendicular to the direction of crack growth. This is coherent with the previous observations, and indicates a rather brittle, intergranular micro-mechanism of propagation.

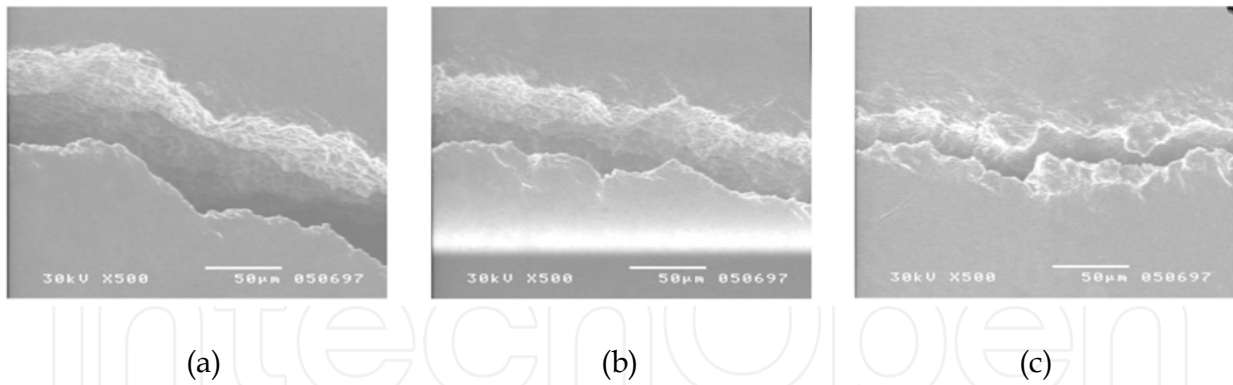


Fig. 16. Stage II crack propagation profiles at constant $R = 0.3$ and applied[average] ΔK equal to: (a) 8.6[16.0] $\text{MPa}\sqrt{\text{m}}$; (b) 11.2[20.8] $\text{MPa}\sqrt{\text{m}}$; (c) 41.0[76.1] $\text{MPa}\sqrt{\text{m}}$.

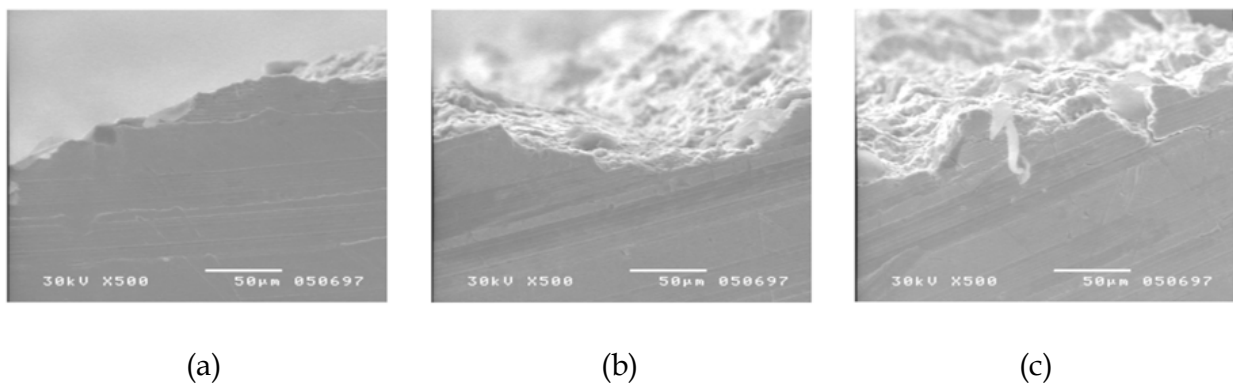


Fig. 17. Stage II crack propagation profiles at constant $R = 0.7$ and applied[average] ΔK equal to: (a) 8.1[45.9] $\text{MPa}\sqrt{\text{m}}$; (b) 12.3[69.7] $\text{MPa}\sqrt{\text{m}}$; (c) 18.7[106.0] $\text{MPa}\sqrt{\text{m}}$.

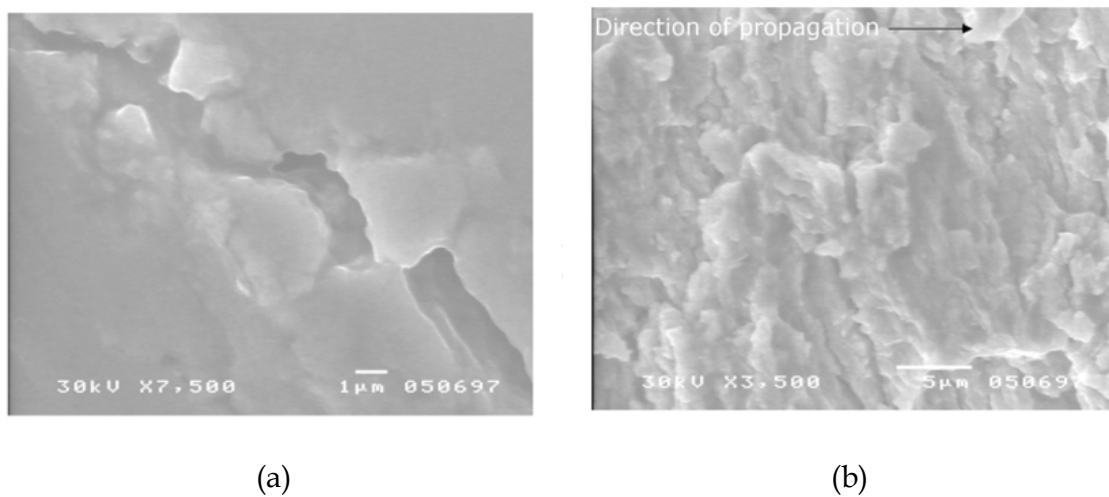


Fig. 18. Crack paths during the threshold regime: (a) intergranular fracture at $R = 0.3$; (b) fracture surface morphology at $R = 0.5$.

6. A model of fatigue crack growth

The ACR model previously discussed is demonstrated as being adequate for interpreting the closure of UFG copper in a stable crack growth (microstructure-independent) regime.

The analysis of the SEM images of a typical crack path such as that reported in Fig. 19, induced the analyst to attempt a model of crack-deflection-induced closure. In fact, the image shows how the crack periodically deflects following a “zig-zag” path, which causes a premature closure mechanism. It’s worth to notice that the direction of main propagation corresponds to the shear plane of the last ECAP passage.

The model proposed by Suresh (1985) has been applied. With the simple geometrical considerations shown in Fig. 19, this model calculates the reduction in the driving force for propagation throughout an effective ΔK_{eff} and a corresponding effective crack propagation rate, as specified in Eq. (14) (see the scheme of Fig. 20 for the symbols):

$$\frac{\Delta K_I}{\Delta K_{eff}} = \left(\frac{D \cos^2(\theta/2) + S}{D + S} \right)^{-1} \left(1 - \sqrt{\frac{\chi \tan \theta}{\chi \tan \theta + 1}} \right)^{-1} \tag{14}$$

$$\left(\frac{da}{dN} \right)_{eff} = \left(\frac{D \cos \theta + S}{D + S} \right) \left(\frac{da}{dN} \right)_L$$

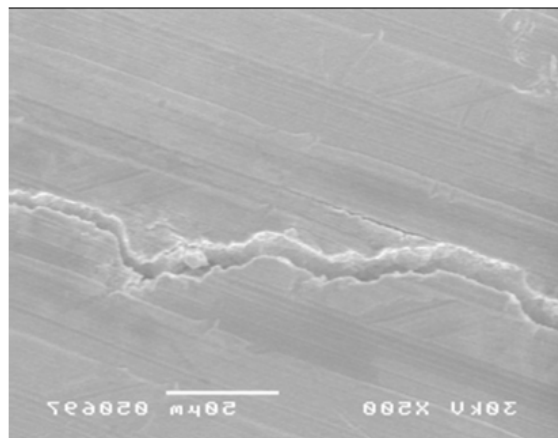


Fig. 19. Propagation path with crack deflections at $R = 0.3$ and applied $\Delta K = 20 \text{MPa}\sqrt{\text{m}}$.

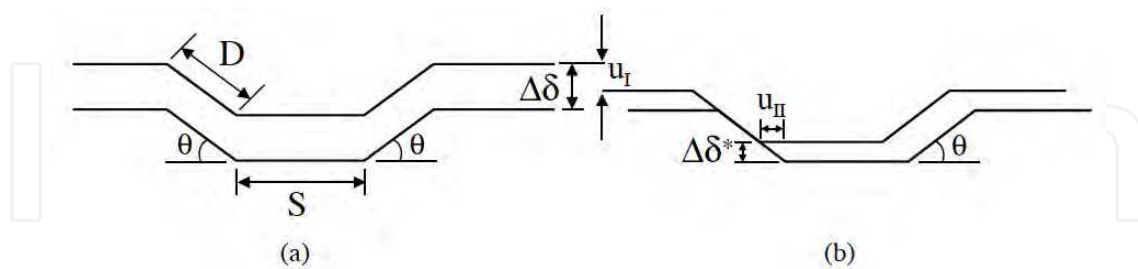


Fig. 20. Scheme of a periodically deflected crack: (a) opened state at the peak load: S is the straight length, D the deflected length, θ the deflection angle, $\Delta\delta$ the CTOD; (b) at the first point of contact upon unloading: u_I and u_{II} are the surface mismatches, $\Delta\delta^* = u_{II} \tan \theta$ is the closure CTOD.

The elaboration of the experimental points via this model is depicted in Fig. 21. Propagation points at the near-threshold regime are well interpreted by the model of Eq. (14), fitted with the following parameters: $D = S = 30 \mu\text{m}$; $\theta = 26^\circ$; $\chi = 0.09$ at $R = 0.1$, $\chi = 0.0125$ at $R = 0.3$, $\chi = 0.0083$ at $R = 0.5$, $\chi = 0.0$ at $R = 0.7$. It is clear that the ACR model rationalises the R -ratio

effect in FCG stage II with a discrete approximation, while it fails when applied to the threshold regime, where evidently the role of the microstructure is of greater importance.

On the other hand, the model of the deflection of the crack rationalises well the closure mechanism occurring when the growth rate is very low. The mismatch parameter χ , which measures the level of crack closure, diminishes when the load ratio (or K_{max}) increases; this is due to the increase in fracture surface separation with an increasing R . The adopted values of the mismatch parameter u_I and u_{II} , however, indicate that a relatively few number of grains are involved in the process at a slow crack growth rate.

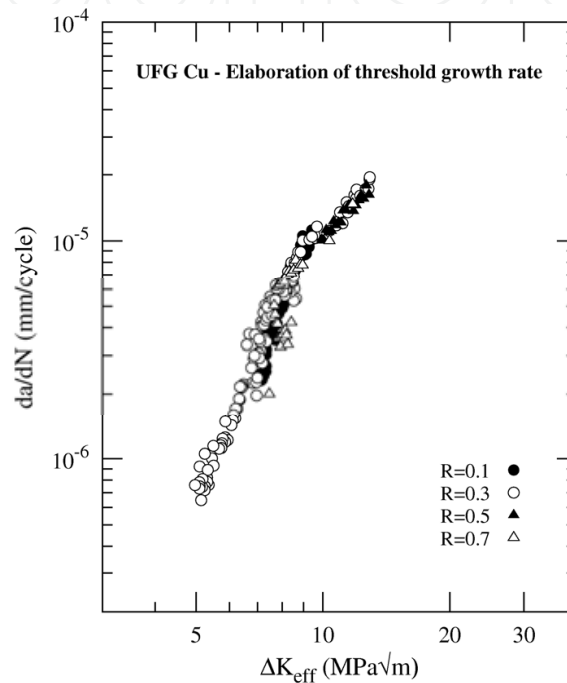


Fig. 21. Crack closure elaboration at stage II (left) and stage I (right).

The mechanism of propagation at high crack growth rates, and the interrelationship with the ultrafine structure remains to be fully investigated. As already evidenced, the fractographic analysis conducted on several crack surfaces from the SEM microscope, revealed an increasing tortuosity and fragmentation of the crack with an average ΔK , over all the R -ratios. The profile morphology at the highest loads shows bifurcation, multi-cracking and branching of the main crack, and several small secondary cracks appearing in perpendicular and parallel directions with respect to the main crack direction, and even at some distance from it. Microcracks generating to accommodate excessive strains in the crack vicinity cause a decrease in the strain hardening capability due to severe grain refinement. Nevertheless, the branching mechanism may be directly responsible for the insensitivity toward crack propagation found at the stable FCG rate. Indeed, during stage II propagation, the FCG rate diminishes when the R -ratio (i.e. K_{max}) increases, in other words when branching becomes more evident. Effectively, crack branching would reduce the mode I crack driving force and has been known to play a significant role in crack retardation. Recently, in a work on finite element modelling of fatigue crack branching, it has been shown that the near-tip SIF range was significantly reduced due to crack branching

(Meggiolaro et al., 2005). The crack tip stress shielding introduced by crack branching could be considered to be the reason for the lower crack growth rates observed, definitely explaining the FCG behaviour of the UFG structure witnessed.

7. Conclusions

The experiments have shown that the resistance to the crack propagation in ultrafine-grained copper alloy is not only influenced by the peculiar microstructure and the technological process employed to obtain it, but also by hardening conditions and boundary impurities.

Different crack growth mechanisms are individuated, depending on the crack growth rate (threshold or Paris' regime). In particular, elaboration of the experimental data shows that: 1) a large number of grains are involved in the propagation process; 2) a plastic induced crack closure mechanism is the most probable closure mechanism at high driving force, while a roughness induced crack closure mechanism dominates near the threshold growth rate: this is consistent with the average material grain size.

Finally, the increasing insensitivity toward the fatigue crack propagation shown during the Paris' regime when the R -ratio increases, indicates a mechanism of apparent toughening that can be explained, at least qualitatively, by considering the observed branching of the crack path along the ECAP shear planes.

However, the mechanism of the crack propagation in UFG Cu, and its relation to the microstructure and its changes, up until now have not been sufficiently studied. Further goal-directed investigations are necessary to obtain further knowledge on this issue.

8. Acknowledgements

The author wishes to thank Prof. Ludvik Kunz from the Institute of Physics of Material in Brno, Czech Republic, for providing the material for this research activity, and for the fruitful discussions.

9. Nomenclature

a	crack length (mm)
W	specimen width (mm)
B	specimen thickness (mm)
P	tensile applied load (N or kN)
$C_0 \div C_4$	constants relative to the DSCT geometry
N	number of load cycles
da/dN	crack growth rate (mm/cycle)
K	Stress Intensity Factor (SIF) ($\text{MPa}\sqrt{\text{m}}$)
K_a	applied SIF
ΔK	Stress Intensity Factor amplitude = $K_{\max} - K_{\min}$ ($\text{MPa}\sqrt{\text{m}}$)
ΔK_{th}	Threshold Stress Intensity Factor ($\text{MPa}\sqrt{\text{m}}$)

K_{op}	Stress Intensity Factor necessary to open a crack ($\text{MPa}\sqrt{\text{m}}$)
R	load ratio = K_{min}/K_{max}
C, m	Paris propagation law constants
d_G	average grain size (μm)
$\kappa_{1,2}$	interpolating constants
$\beta_{1,2}$	interpolating constants
A, B	fitting parameters
D, γ	fitting parameters
C_s, C_0, C_i	specimen compliances: secant; above K_{op} ; prior the initiation of crack
ΔK_{eff}	Effective Stress Intensity Factor = $K_{max} - K_{op}$ ($\text{MPa}\sqrt{\text{m}}$)
$(da/dN)_L$	growth rate of a linear undeflected crack (mm/cycle)
S, D, $\theta, \Delta\delta, \Delta\delta^*$	geometrical parameter of crack deflection
u_I, u_{II}	sliding displacement at the crack closure
χ	mismatch parameter = u_{II}/u_I

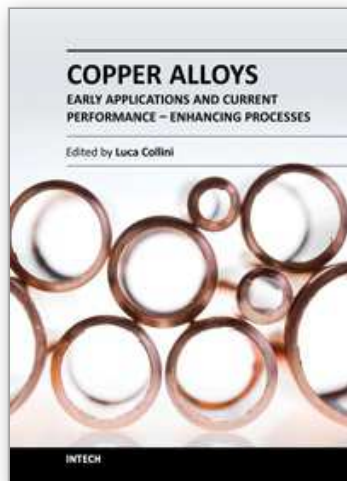
10. References

- Barson J. Fatigue behaviour of pressure-vessel steels. Welding Res Council Bull 1974;194.
- Cavaliere P. Fatigue properties and crack behavior of ultra-fine and nanocrystalline pure metals. Int J Fatigue. 2009;31(10):1476-1489.
- Collini L. Fatigue crack growth in ECAPed commercially pure UFG copper. Proc Eng. 2010a;2(1):2065-2074.
- Collini L. Fatigue crack growth resistance of ECAPed ultrafine-grained copper. Eng Fract Mech. 2010b;77:1001-1011.
- Donald J.K. Introducing the compliance ratio concept for determining effective stress intensity. Int J Fatigue. 1997;19(1), S191-S195.
- Estrin Y., Vinogradov A. Fatigue behaviour of light alloys with ultrafine grain structure produced by severe plastic deformation: an overview. Int J Fatigue. 2010;32(6):898-907.
- Goto M, Han S.Z., Kim S.S., Ando Y., Kawagoishi N. Growth mechanism of a small surface crack of ultrafine-grained copper in a high-cycle fatigue regime. Scripta Mater. 2009;60:729-732.
- Hanlon T., Tabachnikova E.D., Suresh S. Fatigue behavior of nanocrystalline metals and alloys. Int J Fatigue 2005;27:1147-1158.
- Holzapfel C., Schäfer W., Marx M., Vehoff H., Mücklich F. Interaction of cracks with precipitates and grain boundaries: understanding crack growth mechanisms through focused ion beam tomography. Scripta Mater. 2007;56:697-700.
- Höppel H.W., Kautz M., Xu C., Murashkin M., Langdon T.G., Valiev R.Z., Mughrabi H. An overview: Fatigue behaviour of ultrafine-grained metals and alloys. Int J Fatigue. 2006;28:1001-1010.

- Horky J., Khatibi G., Weiss B., Zehetbauer M.J. Role of structural parameters of ultra-fine grained Cu for its fatigue and crack growth behaviour. *J Alloy Compd.* 2011;509S:S323-S327.
- Klesnil M., Lukáš P. Effect of stress cycle asymmetry on fatigue crack growth. *Mater Sci Eng* 1972;9:231-40.
- Kozlov E.V., Zhdanov A.N., Popova N.A., Pekarskaya E.E., Koneva N.A. Subgrain structure and internal stress fields in UFG materials: problem of Hall-Petch relation. *Mater Sci Eng A.* 2004;387-389:789-794.
- Kunz L., Lukáš P., Svoboda M. Fatigue strength, microstructural stability and strain localization in ultrafine-grained copper. *Mater Sci Eng A.* 2006;424:97-104.
- Lugo N., Llorca N., Cabrera J.M., Horita Z. Microstructures and mechanical properties of pure copper deformed severely by equal-channel angular pressing and high pressure torsion. *Mater Sci Eng A.* 2008;477(1-2):366-371.
- Lukáš P., Kunz L. Mechanisms of near-threshold fatigue crack propagation and high cycle fatigue in copper. *Acta Technica CSAV.* 1986;4:460-488.
- Lukáš P., Kunz L., Knésl Z. Fatigue crack propagation rate and the crack tip plastic strain amplitude in polycrystalline copper. *Mat. Sci. Eng.* 1985;70:91-100.
- Lukáš P., Kunz L., Svoboda M. Fatigue mechanism in ultrafine-grained copper. *Kovove Mater.* 2009;47:1-9.
- Marchand N.J., Bailon J.-P., Dickson J.I. Near-threshold fatigue crack growth in copper and alpha-brass: grain-size and environmental effects. *Metall Mater Trans A.* 1988;19(10):2575-2587.
- Meggiolaro M.A., Miranda A.C.O., Castro J.T.P., Martha L.F. Crack retardation equations for the propagation of branched fatigue cracks. *Int J Fatigue.* 2005;27:1398-1407.
- Meyers M.A., Mishra A., Benson D.J. Mechanical properties of nanocrystalline materials. *Prog Mater Sci.* 2006;51:427-556.
- Mughrabi H., Höppel H.W., Kautz M. Fatigue and microstructure of ultrafine-grained metals produced by severe plastic deformation. *Scripta Mater.* 2004;51:807-814.
- Murphy M.C. The engineering fatigue properties of wrought copper. *Fatigue Eng Mater Struct.* 1981;4(3):199-234.
- Suresh S. Fatigue crack deflection and fracture surface contact: micro-mechanical models. *Metall Trans.* 1985;16A:249-260.
- Thompson A.W., Backofen W.A. The effect of grain size on fatigue. *Acta Metal.* 1971;19(7):597-606.
- Valiev R.Z. Structure and mechanical properties of ultrafine-grained metals. *Mater Sci Eng A.* 1997;234-236:59-66.
- Valiev R.Z., Islamgaliev R.K., Alexandrov I.V. Bulk nanostructured materials from severe plastic deformation. *Progr Mat Sci.* 2000;45:103-189.
- Valiev R.Z., Langdon T.G. Principles of equal-channel angular pressing as a processing tool for grain refinement. *Prog Mater Sci.* 2006;51:881-981.
- Vasudevan A.K., Sadananda K., Rajan K. Role of microstructures on the growth of long fatigue cracks. *Int J Fatigue.* 1997;19(1):S151-S159.
- Vinogradov A. Fatigue limit and crack growth in ultra-fine grain metals produced by severe plastic deformation. *J Mater Sci.* 2007;42:1797-1808.

- Wei W., Chen G. Microstructure and tensile properties of ultrafine grained copper processed by equal-channel angular pressing. *Rare Metals*. 2006;25(6): 697-704.
- Xu C., Wang Q., Zheng M., Li J., Huang M., Jia Q., Zhu J., Kunz L., Buksa M. Fatigue behavior and damage characteristic of ultra-fine grain low-purity copper processed by equal-channel angular pressing (ECAP). *Mater Sci Eng A*. 2008;475(1-2):249-256.
- Zhai T., Wilkinson A.J., Martin J.W. A crystallographic mechanism for fatigue crack propagation through grain boundaries. *Acta Mater*. 2000;48:4917-4927.

IntechOpen



Copper Alloys - Early Applications and Current Performance - Enhancing Processes

Edited by Dr. Luca Collini

ISBN 978-953-51-0160-4

Hard cover, 178 pages

Publisher InTech

Published online 07, March, 2012

Published in print edition March, 2012

Copper has been used for thousands of years. In the centuries, both handicraft and industry have taken advantage of its easy castability and remarkable ductility combined with good mechanical and corrosion resistance. Although its mechanical properties are now well known, the simple f.c.c. structure still makes copper a model material for basic studies of deformation and damage mechanism in metals. On the other hand, its increasing use in many industrial sectors stimulates the development of high-performance and high-efficiency copper-based alloys. After an introduction to classification and casting, this book presents modern techniques and trends in processing copper alloys, such as the developing of lead-free alloys and the role of severe plastic deformation in improving its tensile and fatigue strength. Finally, in a specific section, archaeometallurgy techniques are applied to ancient copper alloys. The book is addressed to engineering professionals, manufacturers and materials scientists.

How to reference

In order to correctly reference this scholarly work, feel free to copy and paste the following:

Luca Collini (2012). Fatigue Crack Resistance of Ultrafine-Grained Copper Structures, Copper Alloys - Early Applications and Current Performance - Enhancing Processes, Dr. Luca Collini (Ed.), ISBN: 978-953-51-0160-4, InTech, Available from: <http://www.intechopen.com/books/copper-alloys-early-applications-and-current-performance-enhancing-processes/fatigue-crack-resistance-of-ultrafine-grained-copper-structure>

INTECH
open science | open minds

InTech Europe

University Campus STeP Ri
Slavka Krautzeka 83/A
51000 Rijeka, Croatia
Phone: +385 (51) 770 447
Fax: +385 (51) 686 166
www.intechopen.com

InTech China

Unit 405, Office Block, Hotel Equatorial Shanghai
No.65, Yan An Road (West), Shanghai, 200040, China
中国上海市延安西路65号上海国际贵都大饭店办公楼405单元
Phone: +86-21-62489820
Fax: +86-21-62489821

© 2012 The Author(s). Licensee IntechOpen. This is an open access article distributed under the terms of the [Creative Commons Attribution 3.0 License](#), which permits unrestricted use, distribution, and reproduction in any medium, provided the original work is properly cited.

IntechOpen

IntechOpen